

Covalent Triazine Frameworks
How to cite: *Angew. Chem. Int. Ed.* **2023**, *62*, e202216159

International Edition: doi.org/10.1002/anie.202216159

German Edition: doi.org/10.1002/ange.202216159

Visible-Light-Promoted Switchable Selective Oxidations of Styrene Over Covalent Triazine Frameworks in Water

 Cyrine Ayed⁺, Jie Yin⁺, Katharina Landfester, and Kai A. I. Zhang*

Abstract: Using photocatalytic oxidation to convert basic chemicals into high value compounds in environmentally benign reaction media is a current focus in catalytic research. The challenge lies in gaining controllability over product formation selectivity. We design covalent triazine frameworks as heterogeneous, metal-free, and recyclable photocatalysts for visible-light-driven switchable selective oxidation of styrene in pure water. Selectivity in product formation was achieved by activation or deactivation of the specific photogenerated oxygen species. Using the same photocatalyst, by deactivation of photogenerated H₂O₂, benzaldehyde was obtained with over 99% conversion and over 99% selectivity as a single product. The highly challenging and sensitive epoxidation of styrene was carried out by creating peroxydicarbonate as an initial epoxidation agent in the presence of bicarbonate, which led to formation of styrene oxide with a selectivity up to 76% with near quantitative conversion. This study demonstrates a preliminary yet interesting example for simple control over switchable product formation selectivity for challenging oxidation reactions of organic compounds in pure water.

Introduction

Conversion of basic chemicals by oxidation into high value compounds is an important production step for chemical industries.^[1] Selective oxidation reactions can lead to reactive organic oxygen containing molecules such as alcohols,

epoxides, aldehydes, ketones, and organic acids etc., which can be further used as building blocks during industrial processes. Among those reactions, the selective oxidation of alkenes can form important products as molecular intermediates for the manufacture of perfumes, dyes, agrochemicals, and pharmaceuticals, with aldehyde and epoxide being the most desirable oxidation products.^[2] Most of the reported studies were carried out under thermal conditions. For example, conversion of styrene to benzaldehyde has been reported using [Ru(COD)(L¹)Br₂] with support of NaIO₄ at ambient temperatures.^[3] Recently, a method of photocatalytic oxidation of C–C double bonds was reported using CdS as a photocatalyst.^[4]

Conventional methods for alkene epoxidation, notably styrene, usually involve organic peracids as oxidants.^[5] However, this route led to poor epoxide selectivity with a high yield of undesired side products.^[5d] As one of few examples, Beller et al. reported high epoxidation selectivity on non-terminal alkenes using Co_xO_y-N/C as catalysts under thermal conditions.^[6] Consequently, a number of attempts have been made to substitute the conventional thermal route with the use of environmentally friendly photocatalytic systems for selective oxidation of alkenes. Mainly metal-based photocatalysts have been used, including [Ru(bpy)₃]Cl₂,^[7] copper nanoparticles immobilized on titanium nitride (Cu@TiN),^[8] TiO₂ dispersed on SiO₂,^[9] calcium-modified V₂O₅@SiO₂,^[10] and mixed metal oxides such as WO₃-TiO₂,^[11] in organic solvents with H₂O₂ or O₂ as oxidizing agents. Under these conditions, the selectivity to styrene oxide ranged from 18% to 90%. A few studies later reported the use of Mo-GO/g-C₃N₄ as photocatalysts at elevated temperature (>60°C).^[12] So far, the use of pure organic heterogeneous photocatalysts for selective epoxidation of alkenes is hardly reported.^[13]

Covalent triazine frameworks (CTFs)^[14] have recently emerged as a promising class of pure organic and heterogeneous photocatalysts for visible-light-promoted chemical transformations.^[15] They have been employed as an efficient platform for visible-light-mediated photocatalytic reactions, such as water splitting,^[15b,16] carbon dioxide reduction,^[17] or organic redox reactions etc.^[18] The structural advantages of CTFs lie at the tunable redox potentials via energy band level alignment, low cost and non-toxicity, excellent recoverability, as well as stability during the catalytic processes. As an example for photocatalytic oxidation reactions, CTFs have recently demonstrated nearly quantitative conversion and selectivity in the visible-light-promoted oxidation of alcohols, forming aldehydes as the targeted product.^[19] Nevertheless, control over the product selectivity by CTF-

[*] Dr. C. Ayed,⁺ Prof. K. Landfester, Prof. K. A. I. Zhang

Max Planck Institute for Polymer Research
 Ackermannweg 10, 55128 Mainz (Germany)
 E-mail: kai.zhang@mpip-mainz.mpg.de

J. Yin,⁺ Prof. K. A. I. Zhang
 Department of Materials Science and State Key Laboratory of
 Molecular Engineering of Polymers, Fudan University
 Shanghai 200433 (P. R. China)
 E-mail: kai_zhang@fudan.edu.cn

[†] These authors contributed equally to this work.

© 2023 The Authors. Angewandte Chemie International Edition published by Wiley-VCH GmbH. This is an open access article under the terms of the Creative Commons Attribution Non-Commercial License, which permits use, distribution and reproduction in any medium, provided the original work is properly cited and is not used for commercial purposes.

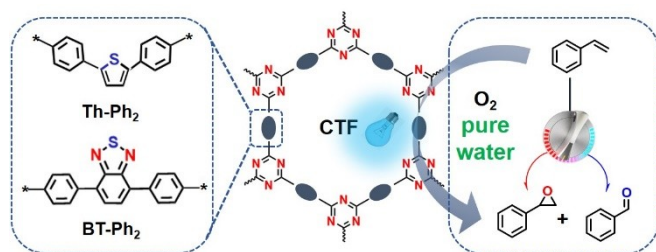
based photocatalytic systems for selective oxidation of alkenes has not yet been documented.

Precise control of product formation selectivity under similar reaction conditions without changing the photocatalyst material remains a large challenge in catalytic research.^[20] For example, König et al. reported switchable photocatalytic debromination reactions on aromatic rings by using different wavelengths as light sources.^[21] Glorius et al. reported that changing the catalyst used for dearomatization of 1-naphthol derivatives alters the products via selective energy transfer of an intramolecular [2+2] cyclization or a higher excitation energy.^[22] For oxidation reactions, photo-generated reactive oxygen species (ROS) such as $\cdot\text{O}^-$, $^1\text{O}_2$, $\cdot\text{OH}$, $\cdot\text{OOH}$, or H_2O_2 etc. play an important role during the oxidation process with different selectivities to products.^[23] Controlled generation or activation of the ROS species provides a useful tool for advancing photooxidative formation of desired products. Therefore, it is urgently needed to investigate specific and controllable activation or deactivation of the ROS for switchable selective oxidation of alkenes.

Herein, we design covalent triazine frameworks (CTFs) as heterogeneous, metal-free, and recyclable photocatalysts for visible-light-driven switchable selective oxidation of styrene in pure water (Scheme 1). Product selectivity was precisely controlled by activation or deactivation of specific photogenerated reactive oxygen species. Using the same CTF as photocatalyst, benzaldehyde was obtained with over 99% conversion and 99% selectivity as a single product by deactivation of photogenerated H_2O_2 . The highly challenging and sensitive epoxidation reaction of styrene was achieved by creating peroxydicarbonate as an initial epoxidation agent in the presence of bicarbonate, leading to formation of styrene oxide with selectivity up to 76% with nearly quantitative conversion. Mechanistic studies using photophysical methods and theoretical calculations demonstrated the favorable reaction pathways under specific control.

Results and Discussion

To gain extra water compatibility and a large accessible surface area, the CTFs were synthesized via solvent-free



Scheme 1. Illustration of the designed covalent triazine frameworks (CTFs) with integrated building blocks for the photocatalytic oxidation of styrene in pure water with switchable product selectivity into benzaldehyde or styrene oxide.

trimerization reaction by polymerizing nitrile-functionalized diphenyl-thiophene (Th-Ph₂) and diphenyl-benzothiadiazole (BT-Ph₂) units as electron donor or acceptor (D-A)-based building blocks on SBA-15 under triflic acid vapor. The obtained CTFs on SBA-15 are referred to as CTF-BT-Ph₂ and CTF-Th-Ph₂. Accordingly, the pure CTFs without SBA-15 support are referred to as Pure-CTF-Th-Ph₂ and Pure-CTF-BT-Ph₂. The aim of choosing Th-Ph₂ and BT-Ph₂ units as building blocks was to investigate the impact of their donor–acceptor backbones on the tunability of product selectivity. The synthetic details are described in the Supporting Information. High-resolution transmission electron microscopy (HR-TEM) showed the presence of ordered mesoporous channels for both samples (Figure 1a and Figure S1a). High-angle annular dark field scanning transmission electron microscopy (HAADF-STEM) illustrated uniform distribution of the elements C, N, and S for CTF-Th-Ph₂ (Figure 1b–e) and CTF-BT-Ph₂ (Figure S1b–e), demonstrating the successful formation of the CTFs on and within the mesopores of SBA-15. Scanning electron microscopy (SEM) images of the materials revealed no aggregation of pure CTF on the surface of SBA-15 (Figure S2). Thermogravimetric analysis (TGA) revealed that both CTFs are stable up to 300 °C under oxygen atmosphere (Figure S3). The X-ray diffraction (XRD) spectrum of Pure-CTF-Th-Ph₂ and Pure-CTF-BT-Ph₂ shows weak peaks at 7°, which correspond to the in-plane pore of the framework, while the broad peaks at 26° correspond to an interlayer distance of the pure CTFs. (Figure S4).

The water contact angle (θ) was recorded to demonstrate a rather hydrophilic nature of the obtained materials with $\theta = 37^\circ$ for CTF-Th-Ph₂ and 42° for CTF-BT-Ph₂ (Figure S5). This ought to enhance their dispersibility and therefore the efficiency of the catalytic reaction in water. The physical properties of the materials are listed in Table S1. Gas adsorption measurements showed typical type-IV adsorption isotherms with noticeable H1-type hysteresis loops in the relative pressure (P/P_0) region of 0.6–0.8 for both CTFs. A linear increase in the absorbed volume at low pressures (<0.3) was observed. These are in accordance with the HR-TEM results, suggesting a typical mesoporous structure (Figure 1a and Figure S1a). The Brunauer–Emmet–Teller (BET) surface areas of CTF-Th-Ph₂ and CTF-BT-Ph₂ were

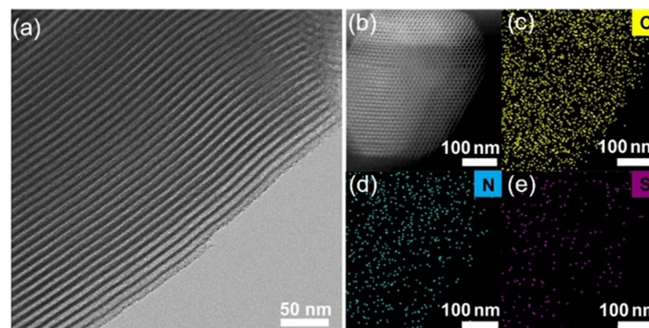


Figure 1. a) HR-TEM and b) HAADF images of CTF-Th-Ph₂ and the corresponding element mapping for c) carbon, d) nitrogen, and e) sulfur.

found to be $486 \text{ m}^2 \text{ g}^{-1}$ and $519 \text{ m}^2 \text{ g}^{-1}$ (Figure S6), with average pore sizes of 7.8 and 7.9 nm for CTF-Th-Ph₂ and CTF-BT-Ph₂, respectively (Figure S7).

Fourier-transform infrared (FTIR) spectra of the two CTFs (without SBA-15) were displayed in Figure 2a. The typical bands at 1348 cm^{-1} and 1503 cm^{-1} can be assigned to the aromatic C–N stretching and breathing modes in the triazine unit. The absence of the band at ca. 2220 cm^{-1} (typical for terminal cyano groups in the monomers) further confirmed the complete trimerization of the nitrile-functionalized monomers.^[24] Solid-state ¹³C cross-polarization magic-angle spinning nuclear magnetic resonance (¹³C/MAS NMR) spectra of CTF-Th-Ph₂ and CTF-BT-Ph₂ revealed a characteristic peak at 167–170 ppm, which can be assigned to sp² carbons in the triazine ring. The rest of the peaks appearing in the range of 120–154 ppm can be ascribed to sp² aromatic carbons of the benzothiadiazole or thiophene (Figure S8).^[25] Further confirmation of the elemental composition of CTF-Th-Ph₂ and CTF-BT-Ph₂ were achieved by X-ray photoelectron spectroscopy (Figure S9).

Ultraviolet-visible (UV/Vis) diffuse reflectance (DR) spectra of CTF-Th-Ph₂ and CTF-BT-Ph₂ showed broader absorption bands in the visible range up to 530 nm (Figure 2b). The optical band gaps of the CTFs were calculated to be 2.55 eV for CTF-Th-Ph₂ and 2.48 eV for CTF-BT-Ph₂ using Tauc plots (Figure 2c). The lowest unoccupied molecular orbital (LUMO) levels were determined to be -0.73 V vs. SCE and -0.78 V vs. SCE by cyclic voltammetry (CV) measurements (Figure 2d). The highest occupied molecular orbital (HOMO) levels of $+1.82 \text{ V}$ vs. SCE and $+1.71 \text{ V}$ vs. SCE were derived from the optical band gaps for CTF-Th-Ph₂ and CTF-BT-Ph₂, respectively. Notably, the reduction of molecular oxygen ($E_{\text{red.}} = -0.56 \text{ V}$ vs. SCE) and the oxidation of styrene ($E_{\text{ox.}} = +0.92 \text{ V}$ vs. SCE) are favored according to redox potentials of both CTFs (Figures S10 and S11). Photoelectrochemical tests were used to illustrate the

photoconversion capability of CTF materials. Figure S12a demonstrates that CTF-Th-Ph₂ has a higher photocurrent response compared to CTF-BT-Ph₂, but also a higher current decay ratio. This photocurrent property can be used to enhance the selectivity of the epoxide products in oxidized styrene. In such cases, the alkene will be easier to oxidize to the epoxide product first, and then with the decline of oxidation ability of CTF-Th-Ph₂, resulting in a difficult transition to the next oxidation state. An electrochemical impedance spectroscopy (EIS) test revealed the photoelectrochemical properties of both CTFs (Figure S12b).

We investigated the selective oxidation of styrene under the irradiation of a LED lamp at 460 nm in pure water as a model reaction. In Table 1, conversion and selectivity of a series of reactions using both CTFs are listed. The main substances identified by gas chromatography–mass spectrometry (GC-MS) are listed in Table S2 for comparison. Figure S13 illustrates a possible mechanism for producing the main products and others. A comprehensive study of the reaction mechanism for switching the product formation selectivity is also shown. Light, CTF, and oxygen are indispensable for the catalytic reaction (entries 1–3). As listed in entries 4 and 5, under standard reaction conditions in pure water, CTF-Th-Ph₂ exhibited a higher substrate conversion of 96 % with a selectivity of 39 % for benzaldehyde. 1-Phenylethane-1,2-diol was determined as the main side product. CTF-BT-Ph₂ showed an increased selectivity of 74 % for benzaldehyde with a conversion of 82 %. No styrene oxide was obtained for both CTFs. We then further analyzed a series of specific scavengers, especially the ones for active oxygen species, and their impact on the product formation selectivity. Using catalase as a H₂O₂ scavenger, benzaldehyde was formed as a single product with almost quantitative conversion and selectivity for both CTFs (entries 6 and 7), indicating a rather negative impact of H₂O₂ for benzaldehyde formation selectivity.

It has been reported that, in the presence of active oxygen species (mostly H₂O₂), bicarbonate anion can be transformed into peroxymonocarbonate (HCO_4^-), which can act as an efficient epoxidation agent.^[26] We then added NaHCO₃ as an additive into the reaction mixture. The selective oxidation of styrene was conducted with a high conversion of 98 % for both CTFs, with CTF-Th-Ph₂ exhibiting a considerably higher styrene oxide selectivity of 76 % (entry 8) than CTF-BT-Ph₂ with 50 % (entry 9). A clear overview of the product formation selectivity for both CTFs is displayed in Figure 3. Only benzaldehyde was detected as a side product for both CTFs. Indeed, the formation of peroxymonocarbonate was confirmed by ¹³C NMR spectroscopy (Figure S14). We then verified the photocatalytic in situ formation of H₂O₂ by the two CTFs via an oxidative process with *N,N*-diethyl-1,4-phenylenediammonium sulfate (DPD) in combination with horseradish peroxidase (POD) in aqueous solution.^[27] As shown in Figure S15d, CTF-BT-Ph₂ appeared to generate a higher H₂O₂ concentration than CTF-Th-Ph₂, although it exhibited a much lower styrene oxide selectivity. To gain a deeper explanation, we further performed electron spin resonance

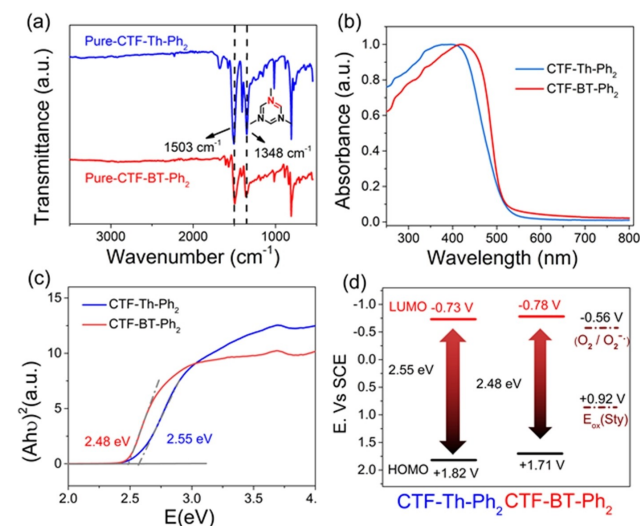
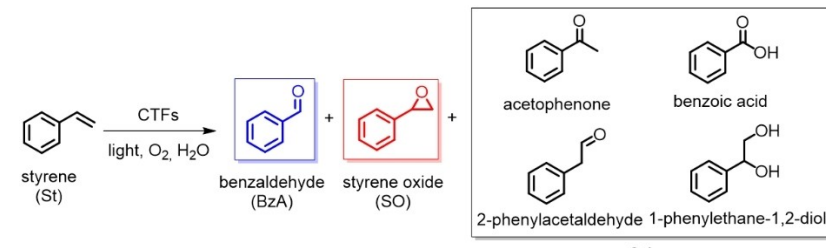


Figure 2. a) Fourier-transform infrared (FT-IR) spectra of the Pure-CTF-Th-Ph₂ and Pure-CTF-BT-Ph₂. b) UV/Vis diffuse reflectance spectra, c) Tauc plot and d) HOMO and LUMO band positions of the CTFs.

Table 1: Photocatalytic switchable selective oxidation of styrene using CTF-based photocatalysts and mechanistic studies under various conditions.^[a]


Entry	Catalyst	Light	O ₂	NaHCO ₃ [mmol]	Scavenger	Conversion [%] ^[b]	Selectivity [%] ^[d]		
							BzA	SO	Others
1	CTF-Th-Ph ₂	–	+	1	–	trace	n.d.	n.d.	n.d.
2	–	+	+	1	–	trace	n.d.	n.d.	n.d.
3	CTF-Th-Ph ₂	+	–	–	–	trace	n.d.	n.d.	n.d.
4	CTF-Th-Ph ₂	+	+	–	–	96	39	n.d.	61
5	CTF-BT-Ph ₂	+	+	–	–	82	74	n.d.	26
6 ^[d]	CTF-Th-Ph ₂	+	+	–	catalase	99	99	n.d.	trace
7 ^[d]	CTF-BT-Ph ₂	+	+	–	catalase	99	99	n.d.	trace
8	CTF-Th-Ph ₂	+	+	1	–	98	24	76	86
9 ^[e]	CTF-BT-Ph ₂	+	+	1	–	98	41	50	9
10 ^[f]	CTF-Th-Ph ₂	+	+	–	KI	99	41	n.d.	59
11 ^[g]	CTF-Th-Ph ₂	+	+	1	KI	94	20	41	39
12 ^[h]	CTF-Th-Ph ₂	+	+	–	L-GA	99	36	n.d.	64
13 ^[i]	CTF-Th-Ph ₂	+	+	1	L-GA	99	32	40	28
14	CTF-Th-Ph ₂	+	+	1	catalase	99	30	69	n.d.
15 ^[j]	CTF-Th-Ph ₂	+	+	–	NaN ₃	99	36	28	36
16 ^[k]	CTF-Th-Ph ₂	+	+	1	NaN ₃	99	27	25	48
17 ^[l]	CTF-Th-Ph ₂	+	+	–	isopropanol	97	53	n.d.	47
18 ^[m]	CTF-Th-Ph ₂	+	+	1	isopropanol	99	28	63	7

[a] Standard reaction conditions: styrene (0.2 mmol), CTF (20 mg) in H₂O (5 ml), blue LED lamp (460 nm, 340 mW cm⁻²), 1 atm. O₂, room temperature, 3.5 h. [b, c] Conversion and selectivity determined by GC-MS; n.d.: not detected. [d] Catalase as H₂O₂ scavenger. [e] 1-Phenylethane-1,2-diol as main side product. [f] Potassium iodide (KI) as hole scavenger, 1-phenylethane-1,2-diol as main side product. [g] Potassium iodide (KI) as hole scavenger, benzoic acid as main side product. [h] L-glutamic acid (L-GA) as superoxide scavenger, 1-phenylethane-1,2-diol as main side product. [i] L-glutamic acid (L-GA) as superoxide scavenger, 1-phenylethane-1,2-diol as main side product. [j] Sodium azide (NaN₃) as singlet oxygen scavenger, 2-phenylazetidine as main side product. [k] Sodium azide (NaN₃) as singlet oxygen scavenger, 2-phenylazetidine as main side product. [l] Isopropanol as hydroxyl radical scavenger, 1-phenylethane-1,2-diol as main side product. [m] Isopropanol as hydroxyl radical scavenger, 2-phenylacetaldehyde as main side product.

(EPR) measurements using 5,5-dimethyl-1-pyrroline *N*-oxide (DMPO) as a superoxide and tetramethylpiperidine (TEMP) as a singlet oxygen trapping agent for the two CTFs. As displayed in Figure S15, the signals of the DMPO-[•]O₂⁻ and TEMP-¹O₂ adducts indicated that both CTFs were able to generate similar amounts of [•]O₂⁻, while CTF-BT-Ph₂ generated visibly higher amount of ¹O₂. Indeed, ¹O₂ is more oxidative and reactive than [•]O₂⁻, thus causing an easier further oxidation, leading to more side-product formation and reduced selectivity of the target product. This may explain that, despite the higher oxidative ability of CTF-BT-Ph₂, for formation of sensitive and less stable targeted products such as styrene oxide, a milder photocatalyst such as CTF-Th-Ph₂ is much preferred.

To attain deeper mechanistic insight of the switchable selective oxidation of styrene, we individually blocked the possible photogenerated active species by focusing on CTF-Th-Ph₂ as the photocatalyst. As listed in entries 10–18 in Table 1, the general trend was that addition of scavengers did not have an influence on the overall conversion.

However, the selectivity of the targeted products and side products were considerably affected. Adding KI as a photo-generated-hole scavenger led to 1-phenylethane-1,2-diol (entries 10 and 11). Without the presence of NaHCO₃, L-glutamic acid (L-GA) as a superoxide scavenger led to a slightly reduced 36 % selectivity to benzaldehyde with 1-phenylethane-1,2-diol as the main side product, and styrene oxide was not formed (entry 12). In the presence of NaHCO₃, using L-GA led to a 40 % selectivity to styrene oxide and an increased side product selectivity from 64 % (entry 12) to 24 % (entry 13). Adding catalase as a H₂O₂ scavenger in the presence of NaHCO₃ led to an increased benzaldehyde selectivity of 30 % and a decreased styrene oxide selectivity of 69 % (entry 14), indicating that formation of HCO₄⁻ as an epoxidation reagent was only slight. This is confirmed by the prior literature, in which not only H₂O₂ but also other active oxygen species such as [•]O₂⁻ and ¹O₂ are reported.^[28] Notably, no side product was formed. Using NaN₃ as an ¹O₂ scavenger led to 2-phenylazetidine, which is obviously a side product when azide anion takes part in the

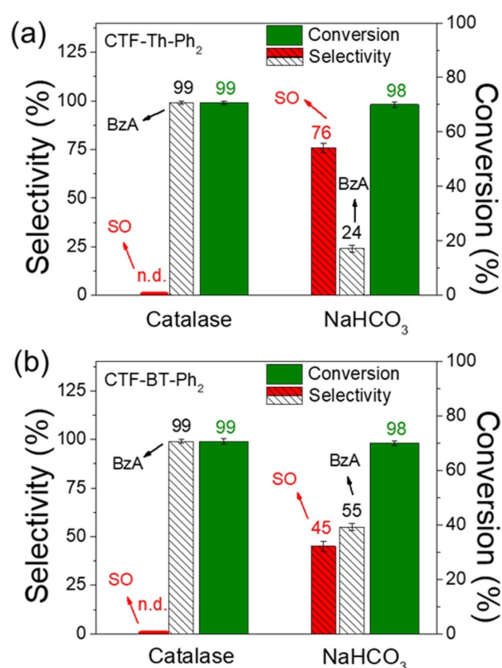


Figure 3. Conversion and selectivity of the switchable photocatalytic oxidations of styrene into benzaldehyde (BzA) or styrene oxide (SO) over a) CTF-Th-Ph₂ and b) CTF-BT-Ph₂ photocatalysts; catalase was used to block H₂O₂ or NaHCO₃ to create peroxymonocarbonate; not determined (n.d.).

reaction. Moreover, styrene oxide product was also detected, which might be generated in the presence of OH⁻ that appears after decomposition of azide (entry 15). In the presence of NaHCO₃, decreased selectivity of both products was determined with increased side-product formation (entry 16). This hints that a balanced amount of ¹O₂ was, indeed, needed for further formation of H₂O₂ and then HCO₄⁻ for the epoxidation reaction. Compared to the basic reaction conditions without any scavenger (entry 4), isopropanol acting as scavenger of hydroxyl radical led to an increased selectivity of benzaldehyde (54 %) and decreased side product formation (entry 17). In the presence of NaHCO₃, the use of isopropanol showed a similar effect compared to catalase (entry 18). The results indicate that the formed amount of hydroxyl radical was likely low and isopropanol scavenges similar radicals such as [•]O₂⁻ etc. In general, NaHCO₃ was necessary for epoxidation of styrene.

Based on the results from the control experiments, we propose individual reaction mechanisms for formation of benzaldehyde or styrene oxide (Figure 4). Figure 4a shows a rather simple reaction pathway towards benzaldehyde, similar to that proposed in the literature.^[29] Under light irradiation, styrene reactant (R2) is oxidized by the photo-generated hole of the CTF and a cationic radical is formed as a transition state (TS2), which is then transformed into the transition state TS3. After releasing formaldehyde as a by-product, the final product benzaldehyde (P2) is formed. The use of catalase ought to prevent undesired side-product formation, as the aqueous reaction favors the formation of other active oxygen species such as H₂O₂ or [•]OH⁻. The

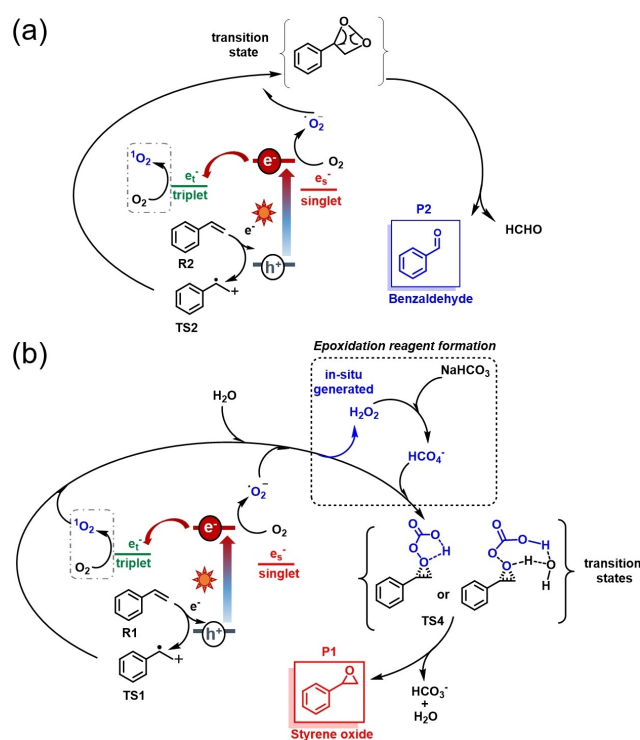


Figure 4. Proposed reaction mechanisms of a) benzaldehyde by blocking the formation of H₂O₂ and b) styrene oxide in the presence of NaHCO₃.

initial steps for styrene oxide formation are similar to that of benzaldehyde (Figure 4b). The decisive step is that, in the presence of NaHCO₃, HCO₃⁻ can be further oxidized into HCO₄⁻, which subsequently reacts with the cationic radical of styrene (TS1), forming transition state (TS4) or its hydrate complex, as reported in the literature.^[30] After losing HCO₃⁻ (or with H₂O), the target product styrene oxide (P1) is finally formed.

In order to elucidate the thermodynamic origin of the two pathways for aldehyde and styrene oxide formation, in-depth density functional theory (DFT) analysis was performed (see the Supporting Information for full computational details; Figure 5). CTF-Th-Ph₂ was taken into account as the photocatalyst during the process. The energies required for favored transition states (TS) and final products were calculated. Superoxide appeared to play a significant role in the formation of benzaldehyde via formation of transition state TS3. For epoxidation, it was clearly shown that the formation of transition state TS4 by HCO₄⁻ is thermodynamically more favorable than the nucleophilic addition by superoxide to TS3. As for the product formation stability, benzaldehyde is more stable than styrene oxide. According to the calculation results, path 1 is thermodynamically more advantageous than path 2, which explains possibly further oxidations towards other side products.

To further demonstrate the general applicability of the CTF-based photocatalyst, various styrene derivatives were tested under the same reaction conditions. The results are listed in Figure S16. Recycling experiments were carried out

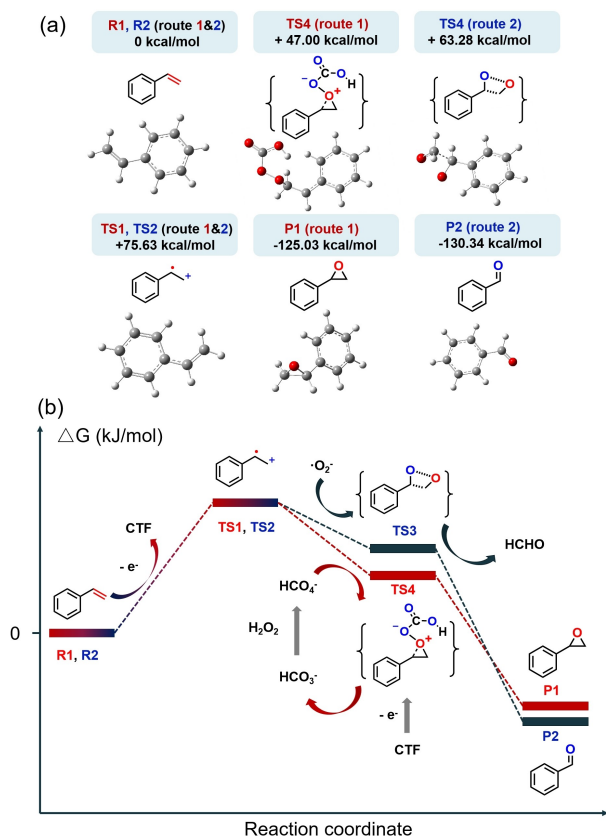


Figure 5. a) An illustration of a simulated molecular structure and of the Gibbs free energy of all compounds in reaction route 1 (R1) and reaction route 2 (R2). b) Analysis of the reaction pathway. The structures of reactants, products, and reaction intermediates were all optimized with density functional theory (DFT) with m062x functional and def2-SVP basis sets. The complex structure of styrene@CTF-Th-Ph₂ was optimized and the excited electronic structures were calculated at the CAM-B3LYP-D3/def2-TZVP level with the time-dependent density functional theory (TDDFT) method.

to investigate the stability and reusability of CTF-Th-Ph₂ as a photocatalyst. Repeat experiments using CTF-Th-Ph₂ are shown in Figure S17. After the photocatalytic reaction, no apparent changes in the UV/Vis DR, FT-IR, and steady-state fluorescence spectrum were observed for either CTF-Th-Ph₂ or CTF-BT-Ph₂, indicating high stability and recyclability of the CTFs (Figure S18).

In addition, Table S4 summarizes the results of styrene oxidation by other photo- and thermocatalysts; this shows that the designed CTFs are comparable to the state-of-art catalysts, and the use of pure water as a solvent is a significant advance.

Photocatalytic reactions are greatly affected by the dispersion of heterogeneous photocatalysts in the catalytic reaction solvent. Poor dispersibility of the pure CTFs without SBA-15 support in aqueous solutions led to decreased photocatalytic efficiency. As listed in entries 1–4 in Table S5 in the Supporting Information, the conversion was determined to be about 20%, which is significantly lower than that of the CTFs on a SBA-15 support. When using acetonitrile as a reaction solvent, the dispersibility of pure

CTFs was increased, leading to increased reaction conversions (entries 5–8 in Table S5). Pure-CTF-Th-Ph₂ showed the highest conversion of styrene of 41% with a selectivity to BzA up to 97%. The general trend was that the overall styrene conversion was increased after prolonging the reaction time to 12 h (Table S5, entries 9 and 10).

Conclusion

In summary, we have developed a useful method for controlled styrene oxidation via photocatalysis in pure water, and with selectivity to particular products. Covalent triazine frameworks (CTFs) were designed as heterogeneous, metal-free, and recyclable photocatalysts. Under similar reaction conditions, switchable product formation selectivity was achieved by activation or deactivation of specific photo-generated reactive oxygen species. Deactivation of photo-generated H₂O₂ led to almost quantitative conversion and selectivity for benzaldehyde as a single product. The highly challenging and sensitive epoxidation of styrene was carried out via formation of peroxydicarbonate as an initial epoxidation agent in the presence of bicarbonate, leading to formation of styrene oxide with selectivity up to 76% with nearly quantitative conversion. As a preliminary yet interesting example, this study demonstrated control over switchable product formation selectivity for challenging oxidation reactions of organic compounds in pure water.

Acknowledgements

C.A. is a recipient of a fellowship through funding of the Excellence Initiative (DFG/GSC 266) of the Graduate School of Excellence “MAINZ” (Materials Science in Mainz). This work is part of the research conducted by the MaxSynBio consortium that is jointly funded by the Federal Ministry of Education and Research of Germany (BMBF) and the Max Planck Society (Grant No. 031A359A). K.A.I.Z. acknowledges the National Natural Science Foundation of China (Grant No. 52173198) for funding. Open Access funding enabled and organized by Projekt DEAL.

Conflict of Interest

The authors declare no conflict of interest.

Data Availability Statement

The data that support the findings of this study are available from the corresponding author upon reasonable request.

Keywords: CTF • Covalent Triazine Framework • Epoxidation • Photocatalysis • Styrene Oxidation

- [1] a) J.-X. Zhu, Z.-C. Chen, W. Du, Y.-C. Chen, *Angew. Chem. Int. Ed.* **2022**, *61*, e202200880; *Angew. Chem.* **2022**, *134*, e202200880; b) A. M. Thayer, *Chem. Eng. News* **1992**, *70*, 27–49.
- [2] a) Y.-C. Lee, K. Kumar, H. Waldmann, *Angew. Chem. Int. Ed.* **2018**, *57*, 5212–5226; *Angew. Chem.* **2018**, *130*, 5308–5322; b) C. C. Chintawar, A. K. Yadav, A. Kumar, S. P. Sancheti, N. T. Patil, *Chem. Rev.* **2021**, *121*, 8478–8558; c) G. Zhan, W. Du, Y.-C. Chen, *Chem. Soc. Rev.* **2017**, *46*, 1675–1692; d) I. P. Beletskaya, C. Nájera, M. Yus, *Chem. Soc. Rev.* **2020**, *49*, 7101–7166.
- [3] P. Daw, R. Petakamsetty, A. Sarbajna, S. Laha, R. Ramapannicker, J. K. Bera, *J. Am. Chem. Soc.* **2014**, *136*, 13987–13990.
- [4] S. Firoozi, M. Hosseini-Sarvari, *Eur. J. Org. Chem.* **2020**, 3834–3843.
- [5] a) G. D. Yadav, A. A. Pujari, *Org. Process Res. Dev.* **2000**, *4*, 88–93; b) M. F. Handley, DOW CHEMICAL CO, United States, **1957**; c) N.-u. H. G. Khan, (IN), Razi Abdi, Sayed Hasan (Gujarat, IN), Kureshy, Rukhsana Ilyas (Gujarat, IN), Singh, Surendra (Gujarat, IN), Ahmed, Irshad (Gujarat, IN), Jasra, Raksh Vir (Gujarat, IN), Ghosh, Pushpito Kumar (Gujarat, IN), United States, **2005**; d) K. T. Nishibe, (JP), Rengakuji, Seiichi (Toyama, JP), Inoue, Masami (Toyama, JP), Ohura, Osami (Fuji, JP), Nitoh, Hirohisa (Fuji, JP), Tokai Denka Kogyo Kabushiki Kaisha (Tokyo, JP), United States, **1992**.
- [6] D. Banerjee, R. V. Jagadeesh, K. Junge, M.-M. Pohl, J. Radnik, A. Brückner, M. Beller, *Angew. Chem. Int. Ed.* **2014**, *53*, 4359–4363; *Angew. Chem.* **2014**, *126*, 4448–4452.
- [7] B. Chandra, K. K. Singh, S. S. Gupta, *Chem. Sci.* **2017**, *8*, 7545–7551.
- [8] Y. Huang, Z. Liu, G. Gao, G. Xiao, A. Du, S. Bottle, S. Sarina, H. Zhu, *ACS Catal.* **2017**, *7*, 4975–4985.
- [9] X. Li, C. Kutal, *J. Mater. Sci. Lett.* **2002**, *21*, 1525–1527.
- [10] G. Wang, S. Zhang, Y. Huang, F. Kang, Z. Yang, Y. Guo, *Appl. Catal. A* **2012**, *413–414*, 52–61.
- [11] M. J. Muñoz-Batista, A. Kubacka, R. Rachwalik, B. Bachiller-Baeza, M. Fernández-García, *J. Catal.* **2014**, *309*, 428–438.
- [12] G. Bian, P. Jiang, F. Wang, Y. Shen, K. Jiang, L. Liu, W. Zhang, *New J. Chem.* **2018**, *42*, 85–90.
- [13] a) C. Sun, H. Liu, *ACS Appl. Polym. Mater.* **2022**, *4*, 5471–5481; b) W. Yu, T. Zhang, Z. Zhao, *Appl. Catal. B* **2020**, *278*, 119342.
- [14] a) H. Dou, M. Xu, B. Wang, Z. Zhang, G. Wen, Y. Zheng, D. Luo, L. Zhao, A. Yu, L. Zhang, Z. Jiang, Z. Chen, *Chem. Soc. Rev.* **2021**, *50*, 986–1029; b) X. Lan, X. Liu, Y. Zhang, Q. Li, J. Wang, Q. Zhang, G. Bai, *ACS Catal.* **2021**, *11*, 7429–7441; c) C. Wang, H. Zhang, W. Luo, T. Sun, Y. Xu, *Angew. Chem. Int. Ed.* **2021**, *60*, 25381–25390; *Angew. Chem.* **2021**, *133*, 25585–25594.
- [15] a) C. B. Meier, R. Clowes, E. Berardo, K. E. Jelfs, M. A. Zwijnenburg, R. S. Sprick, A. I. Cooper, *Chem. Mater.* **2019**, *31*, 8830–8838; b) S. Kuecken, A. Acharjya, L. J. Zhi, M. Schwarze, R. Schomacker, A. Thomas, *Chem. Commun.* **2017**, *53*, 5854–5857; c) F. Niu, L. M. Tao, Y. C. Deng, H. Gao, J. G. Liu, W. G. Song, *New J. Chem.* **2014**, *38*, 5695–5699; d) M. Y. Liu, L. P. Guo, S. B. Jin, B. E. Tan, *J. Mater. Chem. A* **2019**, *7*, 5153–5172.
- [16] a) K. Schwinghammer, S. Hug, M. B. Mesch, J. Senker, B. V. Lotsch, *Energy Environ. Sci.* **2015**, *8*, 3345–3353; b) X. Jiang, P. Wang, J. J. Zhao, *J. Mater. Chem. A* **2015**, *3*, 7750–7758; c) Z. A. Lan, Y. X. Fang, Y. F. Zhang, X. C. Wang, *Angew. Chem. Int. Ed.* **2018**, *57*, 470–474; *Angew. Chem.* **2018**, *130*, 479–483; d) N. Wang, G. Cheng, L. P. Guo, B. E. Tan, S. B. Jin, *Adv. Funct. Mater.* **2019**, *29*, 1904781; e) C. Dai, B. Liu, *Energy Environ. Sci.* **2020**, *13*, 24–52.
- [17] a) C. Yang, W. Huang, L. C. da Silva, K. A. I. Zhang, X. C. Wang, *Chem. Eur. J.* **2018**, *24*, 17454–17458; b) X. Yu, B. Viengkeo, Q. He, X. Zhao, Q. Huang, P. Li, W. Huang, Y. Li, *Adv. Sustainable Syst.* **2021**, *5*, 2100184.
- [18] a) W. Huang, J. Byun, I. Röhrich, C. Ramanan, P. W. M. Blom, H. Lu, D. Wang, L. C. da Silva, R. Li, L. Wang, K. Landfester, K. A. I. Zhang, *Angew. Chem. Int. Ed.* **2018**, *57*, 8316–8320; *Angew. Chem.* **2018**, *130*, 8449–8453; b) L. Guo, Y. Niu, S. Razzaque, B. Tan, S. Jin, *ACS Catal.* **2019**, *9*, 9438–9445; c) J. Byun, K. A. I. Zhang, *Mater. Horiz.* **2020**, *7*, 15–31.
- [19] a) W. Huang, Z. J. Wang, B. C. Ma, S. Ghasimi, D. Gehrig, F. Laquai, K. Landfester, K. A. Zhang, *J. Mater. Chem. A* **2016**, *4*, 7555–7559; b) W. Huang, B. C. Ma, H. Lu, R. Li, L. Wang, K. Landfester, K. A. Zhang, *ACS Catal.* **2017**, *7*, 5438–5442.
- [20] Y. Sakakibara, K. Murakami, *ACS Catal.* **2022**, *12*, 1857–1878.
- [21] I. Ghosh, B. König, *Angew. Chem. Int. Ed.* **2016**, *55*, 7676–7679; *Angew. Chem.* **2016**, *128*, 7806–7810.
- [22] M. J. James, J. L. Schwarz, F. Strieth-Kalthoff, B. Wibbeling, F. Glorius, *J. Am. Chem. Soc.* **2018**, *140*, 8624–8628.
- [23] a) Y.-Z. Chen, Z. U. Wang, H. Wang, J. Lu, S.-H. Yu, H.-L. Jiang, *J. Am. Chem. Soc.* **2017**, *139*, 2035–2044; b) L. Xiong, J. Tang, *Adv. Energy Mater.* **2021**, *11*, 2003216; c) M. Karatok, M. G. Sensoy, E. I. Vovk, H. Ustunel, D. Toffoli, E. Ozensoy, *ACS Catal.* **2021**, *11*, 6200–6209.
- [24] J. Xie, S. A. Shevlin, Q. Ruan, S. J. A. Moniz, Y. Liu, X. Liu, Y. Li, C. C. Lau, Z. X. Guo, J. Tang, *Energy Environ. Sci.* **2018**, *11*, 1617–1624.
- [25] F. Rubio, J. Rubio, J. L. Oteo, *Spectrosc. Lett.* **1998**, *31*, 199–219.
- [26] V. Escande, E. Petit, L. Garoux, C. Boulanger, C. Grison, *ACS Sustainable Chem. Eng.* **2015**, *3*, 2704–2715.
- [27] a) H. Bader, V. Sturzenegger, J. Hoigné, *Water Res.* **1988**, *22*, 1109–1115; b) J. Zou, H. Cai, D. Wang, J. Xiao, Z. Zhou, B. Yuan, *Chemosphere* **2019**, *224*, 646–652.
- [28] E. V. Bakhmutova-Albert, H. Yao, D. E. Denevan, D. E. Richardson, *Inorg. Chem.* **2010**, *49*, 11287–11296.
- [29] a) W. Yu, Z. Zhao, *Org. Lett.* **2019**, *21*, 7726–7730; b) W. Yan, G. Zhang, H. Yan, Y. Liu, X. Chen, X. Feng, X. Jin, C. Yang, *ACS Sustainable Chem. Eng.* **2018**, *6*, 4423–4452.
- [30] C. Bihanic, S. Diliberto, F. Pelissier, E. Petit, C. Boulanger, C. Grison, *ACS Sustainable Chem. Eng.* **2020**, *8*, 4044–4057.

Manuscript received: November 2, 2022

Accepted manuscript online: January 28, 2023

Version of record online: March 1, 2023